

# A novel approach to fabricate uni-directional and branching slender structures using laser-based direct metal deposition

Rajeev Dwivedi, Srdja Zekovic, Radovan Kovacevic\*

*Research Center for Advanced Manufacturing, Southern Methodist University, 1500 International parkway Suite 100, Richardson, TX 75081, USA*

Received 3 March 2006; accepted 15 August 2006

Available online 12 October 2006

## Abstract

The slender structures are identified by a distinctive morphology and large aspect ratio. Contrary to most of the common products, the fabrication of slender structures is usually based on forming operations. For complex shapes; however, machining may be required. Characteristic of machining for a slender structure; however, is the very small ratio of sustained material with respect to the machined material. This paper describes a novel approach to fabricate slender structures using laser-based direct metal deposition (LBDMD) in a layer-by-layer fashion such that the thickness of each layer is infinitesimally small. The existing additive layer-by-layer deposition is guided by  $2\frac{1}{2}$  axis movement and is characterized by intermittent steps. The proposed method, on the contrary, is similar to continuous casting such that the layer thickness can be considered infinitesimally small.

The paper develops a framework for fabrication of slender structures using LBDMD. An algorithm based on geometric reasoning is proposed. Simulations based on Volume Of Fluid (VOF) method and a set of experiments are performed to determine and control various key process parameters. Simulations and experiments performed to determine the a relationship between the material flow rate and corresponding body forces that act on the molten pool as the inclination of substrate changes.

A range of complex geometries that are based on linear as well as nonlinear spatial trajectories are fabricated. The fabricated geometries offer different inclinations as well as material flow rate; hence, support the applicability of proposed method.

© 2006 Elsevier Ltd. All rights reserved.

*Keyword:* VOF; LBDMD; Slender structure; Layered structure; Multi-directional deposition; Silhouette curve

## 1. Introduction

Slender structures are identified by a large ratio between the longitudinal and lateral dimensions. Some of the industrial parts such as structures for aerospace application, aircrafts etc., may be classified as slender structures. Most of the slender structures start with a near net shape of the final part followed by the specialized machining and treating to fabricate the desired shape. The fabrication of slender parts; therefore, requires very a specialized machining setup. The small scale manufacturing of slender parts becomes an expensive and time-consuming venture.

The small-scale fabrication of slender parts involves shaping operations characterized by the removal of a large amount of material to achieve the desired shape. The research

work presented in this paper suggests a technique based on the laser-based direct metal deposition (LBDMD) along multiple axis. The multiple axis metal deposition allows the fabrication of a wide range of complex geometries. Fig. 1 elaborates the method for the fabrication of the slender parts using the laser based direct metal deposition.

The LBDMD is a module of the MultiFab system under development at RCAM, Southern Methodist University, which integrates additive and subtractive manufacturing technologies. The fundamental scheme of LBDMD as described in Fig. 1 includes the delivery of metal powder in a molten pool formed by focusing a continuous wave multi-mode Nd:YAG laser onto a metallic substrate. An inert gas such as Argon acts as the carrier medium for the metal powder as well as protects the molten pool from the surrounding atmosphere. The metal powder melts and adheres to the substrate or the underlying deposit. The fabrication of slender structures is done by the growth of

\*Corresponding author. Tel.: +214 768 4865; fax: +214 768 0812.

E-mail address: [kovacevi@engr.smu.edu](mailto:kovacevi@engr.smu.edu) (R. Kovacevic).

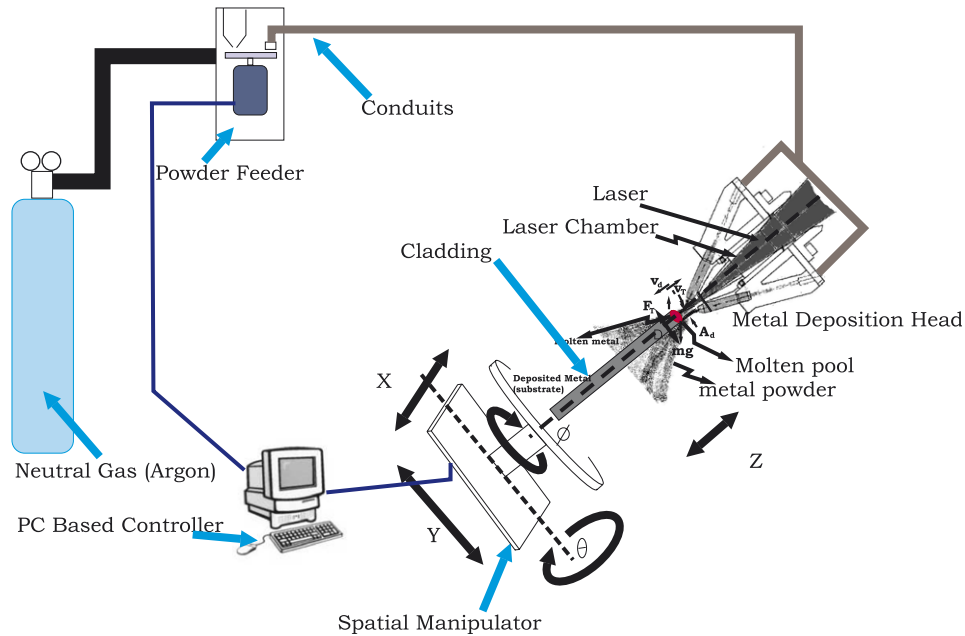


Fig. 1. System for laser-based direct metal deposition.

the part along the direction normal to the molten pool front. The dimensions of the deposition, therefore, depend on the size of the molten pool. A desired geometry is obtained by the relative spatial motion of the substrate and the metal deposition head. The metal powder delivery is controlled by a set of powder feeders. A wide range of the blend of the metal powder composition is obtained by the control of the rate of the metal powder feed from the powder feeders.

The size of the deposition can be controlled by using a set of parameters that includes the laser power, the powder flow rate, etc. It is difficult, however, to manipulate the shape of the molten pool. As described earlier, the slender structure is obtained by part growth along the normal pool front; therefore, the geometry of the molten pool determines the cross-section geometry of the slender structure and, hence, the shape of the structure. In this research, the smaller or the lateral dimension refers to the size of the molten pool that depends on a number of parameters.

In most of the  $2\frac{1}{2}$  layered deposition methods, a layer of finite thickness that is characteristic of the process is deposited. Next, the deposition process is interrupted, and the deposition head moves by a distance along the growth direction in the increment of layer thickness, and then deposition for the next layer starts. A sequence of these steps continues until the top layer is reached. The suggested approach, on the other hand, is similar to the continuous casting. The rate of metal addition and the solidification is done in a coordinated fashion such that, the requirement for deposition process interruption is eliminated. For all practical purposes, the thickness of each layer can be assumed to be infinitesimally small, expressed as

$$\Delta z = \lim_{\Delta t \rightarrow 0} v_{\text{laser}} \Delta t, \quad (1)$$

where  $\Delta z$  is the infinitesimal height of a layer,  $\Delta t$  corresponds to the time interval, and  $v_{\text{laser}}$  is the speed of the metal deposition head.

A detailed account and the advantages of maintaining the infinitesimal thickness is explained in the later sections.

The part accuracy, the reduction in the post processing steps, and the subsequent material wastage are the key issues to fabricate a functional part by Solid Freeform Fabrication (SFF) techniques. Recent approaches for rapid prototyping assisted by CNC machines [1,2], and robot [3–7] have inspired to look forward to the multi-directional deposition for SFF. Contrary to most of SFF techniques that are based exclusively on the  $2\frac{1}{2}$ -axis planar layer deposition approach, the multi-directional approach offers many advantages. The promising results of the laser-based metal powder deposition allows for a material deposition along multiple directions [8–10] and the control of material deposition volume and geometry using different parameters to provide more flexibility, hence, a new direction for direct metal deposition to expand.

Many researchers have described different approaches for the multi-directional material addition for a part fabrication. Singh et al. [7,11] suggested a progressive decomposition of the part into sub-volumes, each of which can be completely built along a certain direction in layers. The elimination of the support requirements, though minimized, cannot be established for all the geometries using this approach. Double-sided layered manufacturing suggested by McMains [12], eliminates the support structure requirement by dividing the part geometry along the parting line, adding material along one direction, flipping the part, and adding material along the second direction. The method of double-sided layered manufacturing applies to a large class of geometries; however, in

intermediate steps, inherent to this method are the human interventions and possible errors due to fixturing. The use of laser chemical vapor deposition (LCVD) and the subsequent process planning based on the use of geometric primitives allows the building of conformal layers [13]. The geometric primitive based process planning and deposition for LCVD, however, is limited to the process.

In a traditional  $2\frac{1}{2}$ -axis planar layered deposition, the slicing of a branching and overhanging structure may yield disconnected islands. The islands usually require supporting structures. A large number of disconnected path elements for different islands render more turning points and path elements, the removal of support structures in the post processing steps adds another set of analysis and planning; therefore, the total time and process complexity is increased.

One of the limitations that may be attributed to the suggested process includes the possible inaccessibility of all the points of a part due to the part geometry. The limitations while governed by the geometry and the material deposition technique employed, depend on the orientation of the part. The choice of a suitable order for the deposition of the layers can eliminate the problems associated with the inaccessibility. A detailed discussion of the method is beyond the scope of this paper; however, the details can be found in a set of papers by the authors [9,10,14].

The key issues associated with the fabrication of slender structures using LBDMD are:

1. The layer thickness is an infinitesimal order, and the deposition is a continuous process, governed primarily by the relative velocity of the metal deposition head and the molten pool.
2. Most of the slender structures follow a complex space trajectory and, therefore, during the deposition process, the underlying support substrate may not be available for all the regions of the slender structure.
3. The geometry of the slender structure is strongly attributed to a set of multiple process parameters that must be controlled suitably.
4. A specified size of the molten pool can support itself by the surface tension; however, the rate of growth of the molten pool must be in an optimal range.

The process planning in the later parts of paper, seeks to address the above-described issues. The first part of the paper investigates the process parameters and their influence on the deposition. The paper also describes an analytical model for the growth of a part, the influence of the rate of metal addition on the rate of part growth, the effect of the gravity vector and surface tension, and the influence of the interface inclination on the deposition. Second, a geometry-based process modeling is described. The algorithm developed on the basis of the model and geometric reasoning and the process planning for the implementation is described in the later section. The paper

concludes with an elaborated discussion of the experimental results.

## 2. A model for SFF based on the LBDMD for slender structures

We develop in this section a formal model for the fabrication of slender structures using the LBDMD process.

### 2.1. Definition of a solid

A solid  $S$  defined in a three-dimensional (3D) Euclidian space is a closed subset of  $R^3$  such that it is identified by its *interior* defined as  $p \in S$  and its *exterior*,  $p \notin S$ , is the complement. The boundary of the solid is defined by the region  $p \in \partial S \subset S$  that is the subset of solid where any neighborhood contains non-members.

### 2.2. Solid as an approximation of layered structure

As described earlier in the SFF method, a part is fabricated by layered deposition of material. The layer exhibits a uniform cross-section. A mathematical model for the layer can be described as the sweep of the area  $A$  along the vector  $\hat{v}_g$  where the subscript  $g$  corresponds to the growth direction.

Let us define the fabrication of the part by SFF as a set of entities *swept* along a growth direction:

$$P = \bigcup_{i=1}^n A_i \oplus \hat{v}_g, \quad (2)$$

where  $\oplus$  represents the Minkowski sum and  $A_i \oplus \hat{v}_g$  is the translation of  $i$ th cross-section  $A_i$  along the vector  $\hat{v}_g$ .

For a multi-directional deposition, the growth direction vector is different for different regions; therefore, the above model is expressed as

$$P_{\text{multi-direction}} = \bigcup_{i=1}^n \bigcup_{j=1}^m A_j \oplus \hat{v}_i, \quad (3)$$

where the variables  $m$  and  $n$  correspond to the number of layers and the number of regions with distinct growth vectors, respectively.

The above representation, however, may be modified for the SFF for the slender structures. A slender structure of a varying cross-sectional area can be fabricated using this technique. The cross-sectional area of the structure can be varied by changing the process parameters.

The infinitesimal volume of material that is added onto substrate in a small amount of time is given by

$$\Delta P = A(t)v_{\text{laser}}(t)\Delta t, \quad (4)$$

where  $A(t)$  is the cross-sectional area of the deposit at the time instant  $t$ ,  $v_{\text{laser}}(t)$  is the velocity of the deposition head at time instant  $t$ .

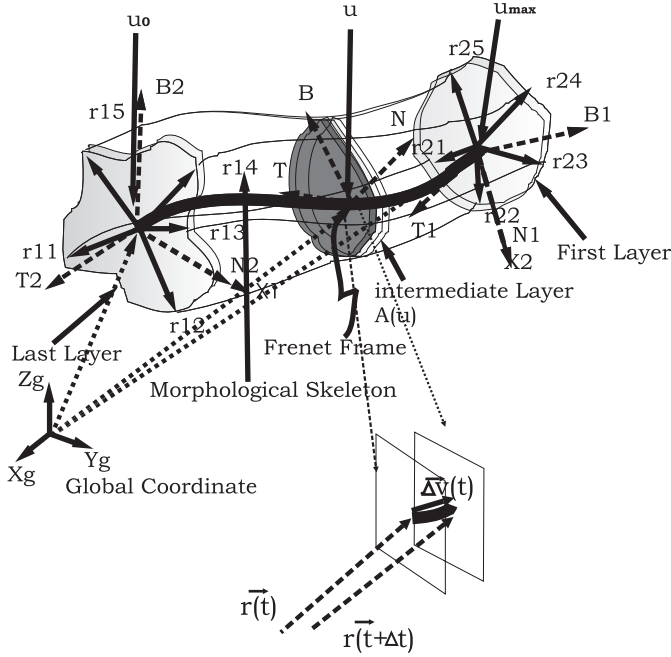


Fig. 2. Generalized cylinder parametric  $u$ -coordinates and Frenet Frame.

For a subregion of the part being fabricated, the solid generation is expressed by

$$P = \int_{u_0}^{u_{\max}} A(u) du, \quad (5)$$

where  $u$  refers to the axial parametric coordinate along the longitudinal direction (Fig. 2).  $A(u)$  expresses the area as a function of the parametric coordinate. The  $u_0$  and  $u_{\max}$  refer to the initial and final coordinates along the parametric axis. We may attribute the Frenet Frame or a local coordinate system at the point where the metal deposition takes place (Fig. 2).

The fabrication of a solid having branches can, therefore, be expressed by

$$P_b = \sum_{i=1}^b \int_{i_{u_0}}^{i_{u_{\max}}} A_i(u) du, \quad (6)$$

where  $P_b$  is the branched solid, and  $b$  is the maximum number of branched subregions in the solid. For the actual implementation, we may attribute time as a parameter for the parametric coordinate  $u$  at an instant  $t$ , such that

$$u(t) = f(p) \delta \left( t - \sum_{j=0}^p \Delta t_j \right), \quad (7)$$

where  $p$  is a time interval over which the process parameters are constant, and  $f(p)$  is the function representing parametric curve. The  $\delta()$  is the impulse function. The primary idea is to fabricate a part by dividing the fabrication process into a set of time steps in order to generate a CNC code.

### 2.3. Generalized cylinder

The generalized representation (Fig. 2) of a solid implies the object representation by a set of two arbitrary curves. The first curve is a cross-section ( $A(u)$ ), defined by a planar closed 2D contour enclosing a finite area. The second curve is an axis curve, ( $C(u)$ ) which is a 3D trajectory in the  $E^3$ . The  $u$  refers to a parameter that varies as

$$i_{u_{\min}} \leq i u \leq i_{u_{\max}} \quad (8)$$

such that the input ( $C(u)$ ) implies an affine transformation of the section as a function of the parameter  $u$ . Parameter  $i$  is identified by the distinct region being represented by the generalized cylinder. The solid is expressed as an infinite set of tuples  $\gamma_j = \langle p_j, v_j \rangle$ , where a point  $v = (x, y)$  in the ( $C(u)$ ) is mapped to  $p$ , a point in the volume domain, expressed as

$$\gamma(u) = C(u) + A(u) \cdot e(u), \quad (9)$$

where  $e(u) = (\hat{e}_x(u), \hat{e}_y(u))$  corresponds to the Frenet Frame, a local coordinate system in the 3D space.

The solid, therefore, is expressed as

$$\Gamma(u) = \{\gamma_1, \gamma_2, \dots\}. \quad (10)$$

The Frenet Frame (Fig. 2) is determined by the instantaneous tangent vector of the trajectory curve. Let the trajectory curve be expressed in terms of the parameter  $u$  as

$$C(u) = C_x(u)\hat{e}_1 + C_y(u)\hat{e}_2 + C_z(u)\hat{e}_3, \quad (11)$$

where  $\hat{e}_1(u)$ ,  $\hat{e}_2(u)$  and  $\hat{e}_3(u)$  are obtained as

$$\hat{e}_1(u) = \frac{C(u)'}{|C(u)'|}, \quad (12)$$

$$\hat{e}_3(u) = \frac{\hat{e}_1(u) \times C(u)''}{|\hat{e}_1(u) \times C(u)''|}, \quad (13)$$

$$\hat{e}_2(u) = \hat{e}_3(u) \times \hat{e}_1(u). \quad (14)$$

The process of metal addition is viewed as the traversal of the metal deposition head along a trajectory (the tool path) by an area (the shape of molten pool) to generate the layer as a combination of the generalized cylinders. The trajectory defined by the tool path is a set of piecewise linear and non-linear functions.

### 3. Steps of process planning

The process planning steps to fabricate a slender structure start with the computer model of the part. Then the morphological skeleton of the part is extracted. The extraction of skeleton from its computer model is relatively complex and time consuming process for many solids; however, for the slender structures it is relatively simple and accurate. Owing to the geometrical morphology of the part, the step for the extraction of the skeleton from the solid model of the part may be eliminated, and the part may be expressed directly as a space trajectory.

In the second step, the spatial trajectory is subdivided into different regions, and the orientation vectors for each region is determined. The hierarchy of the order of regions to be fabricated is assigned in the next step. In the final step, machine inputs are generated for the coordinated orientation of the substrate and the metal deposition head.

### 3.1. An analytical model for the growth at the interface during part build and the influence of parameters

The geometry of the slender part fabricated by the LBDMD process depends on various factors such as the relative orientation of the molten interface with respect to the metal deposition head and the size of the molten interface. There are two different ways to deposit the metal. The first method suggests the orientation of the substrate such that the molten metal is supported by the material underneath. For the metal deposition technique based on the provision of the substrate underneath the layer added at the instant, a mathematical relationship may be expressed as

$$\hat{n}_a \cdot \hat{g} = -1$$

such that  $\Delta x = 0$ ,  $\Delta y = 0$ ,  $\Delta z = \text{layer height}$ , (15)

where  $\hat{n}_a$  is the unit normal vector for the instantaneous area of the slice. The  $\hat{g}$  is the unit vector along the gravity axis. The reorientation of every layer is done in such a way that the layer being deposited is supported by the previous layer.

In the second approach, there is no requirement for the support structure underneath. Eq. (16) describes the metal deposition taking place along an arbitrary orientation:

$$1 \geq \hat{n}_a \cdot \hat{g} > -1$$

such that  $\Delta x = 0$ ,  $\Delta y = 0$ ,  $\Delta z = \text{layer height}$ . (16)

The influence of gravitational force on the metal powder particles is negligible compared to the aerodynamic drag of carrier gas. This drag provides a characteristic ability to shoot material in LBDMD along any direction. The deposition of material is controlled such that the support requirement for overhanging structures can be avoided. The force due to surface tension, acting on the molten pool, can counter the gravitational force. However, the accessibility of the point of metal deposition is limited by the configuration and geometry of the substrate-holder-manipulator, and the metal deposition head. Also, due to the mode of powder delivery, the probability of the metal powder to reach the molten pool is more in the domain, corresponding to  $0 \geq \hat{n}_a \cdot \hat{g} \geq -1$ ; however, the part requires a suitable orientation in order to deposit metal. Therefore, the process planning, primarily, focusses for the domain defined by  $0 \geq \hat{n}_a \cdot \hat{g} \geq -1$  such that  $\Delta x \geq 0$ ,  $\Delta y \geq 0$ ,  $\Delta z \geq 0$ .

The approach for fabrication of slender structures using the LBDMD process combines different methods to

fabricate complex shapes to address the issues pertaining to:

1. Accessibility.
2. Deposition rate.

One of the main advantages of sustaining the molten interface over the entire deposition process is the uniformity of microstructure and fully dense structures.

### 3.2. An analytical model for the interface growth on slender structures

Similar to most of the  $2\frac{1}{2}$ -axis deposition methods, the slender structures are formed by generating a molten volume, then adding metal powder to the molten volume; however, the part growth is a continuous process. The desired shape of the slender structure is obtained by the relative orientation and relative motion of the molten volume and the stream of metal powder.

A set of forces act on the molten volume of metal. Depending upon the orientation of molten metal volume and the supporting substrate, the forces may aid in detaching or retaining the molten metal onto the substrate. The forces are listed down as [15] follows:

- gravitational force ( $F_g$ ),
- aerodynamic drag force ( $F_{aero}$ ),
- inertial force ( $F_i n$ )
- Marangoni effects due to flow inside the molten volume ( $F_{mar}$ )
- surface tension ( $F_\gamma$ )
- vapor jet force ( $F_{Vjet}$ )

The order of the force due to inertia and the Marangoni effects is much smaller than other forces, therefore neglected. The influence of various other factors has been discussed in detail and may be found in a set of papers by authors [16,17]. Of the set of forces, the gravitational  $F_g$  and aerodynamic force  $F_{aero}$  forces aid the detachment of the molten metal volume when the substrate is inclined at a non-zero inclination with respect to the gravity vector. The force due to surface tension, on the other hand, prevents the detachment. For a given inclination, a suitable rate of metal deposition can be determined such that the forces acting on the molten metal volume are balanced. We performed a set of numerical simulations to estimate the shape and size of the largest molten volume that can be generated using a set of process numerical parameters.

A preliminary set of simulations were performed towards the modeling of the growth of the molten pool using the Volume Of Fluid (VOF) approach. The framework for the implementation of the VOF is provided by FLOTRAN, VOF [18]. The simulation results suggest the desired rate of material deposition for a different size of the molten pool and the inclination of the interface such that the force due

to the surface tension can counter the gravitational force acting on the molten metal as described in Fig. 1.

In the VOF approach, the evolution of a free surface is expressed by

$$\frac{\partial \chi}{\partial t} + \vec{U} \cdot \nabla \chi = 0, \quad (17)$$

where  $\chi$  is the volume fraction of fluid. The VOF approach is based on the following assumptions:

1. A free surface refers to an interface between a gas and a liquid where the difference in the densities between the two is quite large.
2. Due to a low density, the inertia of the gas is usually negligible.
3. The free surface is simply modeled as a boundary with a constant pressure.
4. The location of free surface is determined based on the concept of a fractional VOF.
5. A unity value of the volume fraction corresponds to a full element occupied by the fluid; a zero value indicates an empty element containing no fluid; whereas, a fractional value corresponds to partial or free surface.

The implementation of the VOF in this work is done using the Computational Lagrangian–Eulerian Advection Remap-Volume of Fluid (CLEAR-VOF) algorithm described as:

*Step 1:* Move the fluid portion of an element in a Lagrangian sense.

*Step 2:* Compute how much of the fluid remains in the home element, and how much of it passes into each of its neighboring elements.

The incorporation of the effect of surface-tension is done using the continuous surface force method expressed by

$$\vec{f}_s = \sigma \kappa \hat{n} + \nabla_f \sigma, \quad (18)$$

Where  $\vec{f}_s$  is the surface force,  $\sigma$  the surface tension coefficient,  $\kappa$  the surface curvature,  $\hat{n}$  the unit normal vector and  $\nabla_f$  the surface gradient. Determination of the individual parameters is done using the following set of relationships:

Surface curvature:

$$\kappa = -\nabla \cdot \hat{n} = \frac{1}{|\vec{n}|} \left[ \left( \frac{\vec{n}}{|\vec{n}|} \cdot \nabla \right) |\vec{n}| - (\nabla \cdot \vec{n}) \right], \quad (19)$$

Surface normal:

$$\hat{n} = \frac{\vec{n}}{|\vec{n}|} = \frac{\nabla F}{|\nabla F|}, \quad (20)$$

Surface gradient:

$$\nabla_{\hat{t}} = \hat{t}(\hat{t} \cdot \nabla), \quad (21)$$

where  $\hat{t}$  is the unit tangent vector at the surface.

The continuous surface force is formulated into the volumetric force by

$$\vec{F}_s = \vec{f}_s \delta_s \frac{F}{\langle F \rangle}, \quad (22)$$

where  $\langle F \rangle$  is averaged volume fraction across the interface and  $\delta_s$  is the surface delta function expressed as

$$\delta_s = |\vec{n}| = |\nabla F|. \quad (23)$$

The boundary conditions for the VOF analysis are described in Fig. 3. The set of parameters used is as follows:

- acceleration due to gravity ( $g$ ) = 9.81 m/s<sup>2</sup>,
- molten metal density ( $\rho$ ) = 7000 kg/m<sup>3</sup>,

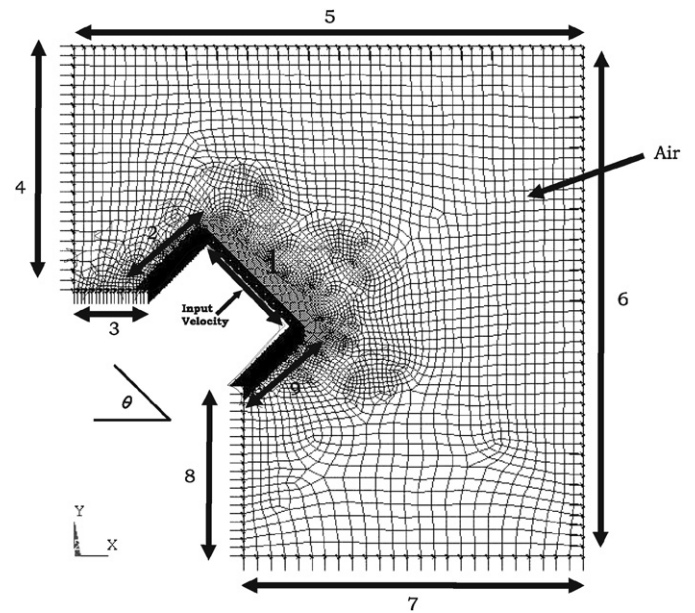


Fig. 3. The boundary conditions and the mesh. For the face 1 the velocity components of flow  $v_x$  and  $v_y$  are non-zero; whereas, for the rest of the faces 2–9, the velocity components have zero values.

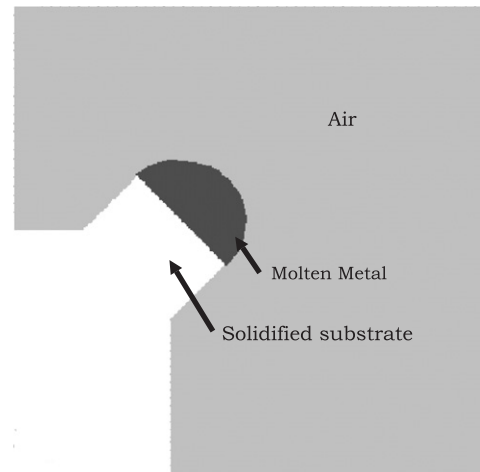


Fig. 4. The VOF simulation result for droplet formation corresponding to the molten face inclination,  $\theta = 45^\circ$ .

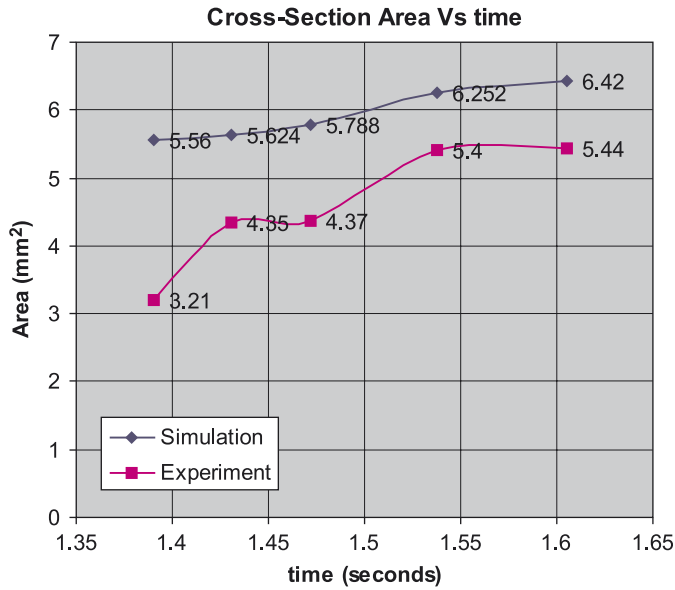


Fig. 5. The area of largest cross-section at the molten interface obtained by simulation and experiment.

Table 1  
Time before which flow of molten metal starts for different inclination of molten pool

Serial no./ parameter	Angle ( $\theta$ ) (rad)	Time (s)	Area (mm <sup>2</sup> )	Measured area (mm <sup>2</sup> )
1	$\pi/12$	1.605	6.420	5.44
2	$\pi/6$	1.538	6.252	5.4
3	$\pi/4$	1.472	5.788	4.37
4	$\pi/3$	1.431	5.624	4.35
5	$5\pi/12$	1.390	5.560	3.21

- coefficient of viscosity ( $\mu$ ) = 5.7,
- molten face inclination angle ( $\theta$ ) = 45°.

The simulation results exhibit a correlation between the rate of metal deposition and the angle of inclination of the interface. Fig. 4 depicts the molten pool formed by the VOF simulation for the above-described set of parameters. However, due to various limitations attributed to the modeling tool, there is a difference in the simulation and the experimental observation.

Fig. 5 describes a plot of the area obtained by simulation and experimental measurement summarized in Table 1. The areas correspond to the largest cross-section area along the molten interface before the dripping of metal starts.

### 3.3. Parameters affecting the size of molten pool and the part growth

The material deposition in SFF methods is a sequential time dependent process. The material deposition head follows a spatial trajectory and delivers the material. Yet another set of SFF processes are based on the traversal of

the source of energy or a binding agent onto a layer of material that has already been laid on a platform or the previous layer. However, we can say that common to all the methods is a time invariant finite amount of material deposition over per unit time, expressed as

$$\frac{dm}{dt} = \rho A(v_g(t) - v_{\text{laser}}(t))\eta, \quad (24)$$

where  $dm/dt$ ,  $v_g(t)$ ,  $v_{\text{laser}}(t)$ ,  $\rho$ ,  $\eta$  and  $A$  correspond to the metal deposited per unit time, velocity function of metal gas mixture, velocity function of the movement of the deposition/energy head, density of the powder flow, the volume factor of the gas powder in gas powder mixture, and the lateral area of the molten pool, respectively.

The size of molten pool, in essence the diameter  $D_{\text{mp}}$  depends mainly on the laser power  $P$ , the rate of deposition of the volume of material  $\dot{V}_m$ , the relative velocity of the instantaneous substrate and the metal deposition head, the initial rate of volume flow  $\dot{V}_{\text{init}}$ , and the  $g$ -vector  $\vec{g}$ :

$$\dot{V}_m = \eta(d)\dot{V}_{\text{init}}, \quad (25)$$

where  $\eta(d)$  is a factor that determines the fraction of actual metal powder that reaches to the molten pool, and depends on the distance between the metal powder exit point and the distance of the exit point from the molten pool.

The rate at which the metal deposition  $\dot{V}_{\text{dep}}$  onto the substrate takes place is given by

$$\dot{V}_{\text{dep}} = \dot{V}_m \pi D_{\text{mp}}. \quad (26)$$

A set of experiments, explained in the later sections, are performed towards the estimation of the influence of the parameters.

### 3.4. System used for LBDMD

The process planning is implemented on a multiple degree of freedom machine, *MultiFab* being developed at the Research Center for Advanced Manufacturing (RCAM), at Southern Methodist University. *MultiFab* provides a high concentration of a variety of material deposition and machining processes for the fabrication and repair of parts. A more detailed description of the system is available in [19]. A 5-axis CNC machine with a 16-tool tool changer is used for intermediate and/or final machining of the part. The support platform that holds the substrate is a 4-axis manipulation table consisting of a rotary and tilt axis as well as two perpendicular linear stages. A further 5<sup>th</sup> axis is provided by the vertical movement of machining head. The schematic figure of the machine kinematics is explained in Fig. 1. The metal deposition head is mounted at the end effector of a 6-axis robot and is manipulated in the space for multi-axis metal deposition. The LBDMD process is characterized by the ability to build finer geometrical features with a smaller heat-affected zone, less porosity, multiple material deposition, better control of the material properties, and the possibility to deposit metal powder in any direction.

### 3.5. Derivation of the machine kinematics based on the part geometry

The metal deposition is primarily governed by the orientation and location of the molten metal front. A parametric coordinate system may be attributed to the molten metal front. The location and orientation of the molten metal front is governed by the tilt along tilt axis ( $\theta_t$ ), the rotation along the rotational axis ( $\phi_r$ ) and displacements along the  $x$ ,  $y$ , and  $z$  (see Fig. 1). Key to uniform deposition is the suitable control of the machine kinematics and the process parameters. For a geometry  $G(u)$  defined by the parameter  $u$  for the generalized cylinder, the machine parameters are obtained by the following relationship:

$$\begin{pmatrix} x(u) \\ y(u) \\ z(u) \\ \theta_t(u) \\ \phi_r(u) \end{pmatrix} = M_{\text{trans}} G(u), \quad (27)$$

where the  $M_{\text{trans}}$  is the cumulative transformation matrix that relates the molten metal front to the global coordinate system. For, global coordinate system expressed by  $C_G$ , the cumulative transformation matrix is obtained by the following relationship:

$$M_{\text{trans}} = A_{G2} A_{23} A_{34} \dots, \quad (28)$$

where  $A_{ij}$  corresponds to the transformation matrix of a reference system  $j$  with respect to  $i$ . The extreme values, the possible collision, and the limited work envelope of the tilt and rotary axis may not allow the fabrication of very complex parts; however, by introducing the robot as a manipulator for the metal deposition head, it is possible to make more complex parts. The relative orientation of the metal deposition head and the table for the substrate, allows the introduction of another set of configurations. Let us attribute a coordinate system  $C_M$ , characterized by a set of parameters  $x_M$ ,  $y_M$ ,  $z_M$ ,  $\theta_M$  and  $\phi_M$ , to the focus point of the metal deposition head. Then the coordinate system  $C_G$  is expressed by

$$C_G = A_{GM} \begin{pmatrix} x_M \\ y_M \\ z_M \\ \theta_M \\ \phi_M \end{pmatrix}, \quad (29)$$

where the matrix  $A_{GM}$  depends on the relative configuration of the focal point of metal deposition head and the absolute coordinate system. Hence, the variants of the  $A_{GM}$  enhance the total number of possible configurations.

### 3.6. Decomposition of a slender solid into subregions

A large class of slender structures comprise of the piecewise linear nature of parametric curve for the skeleton curve. In this section, we introduce a method to reduce the number of process variables. The method divides a solid into a set of subregions. Each subregion is identified by a vector, such that the values  $\theta_M$  and  $\phi_M$  as described in the previous sections are held constant. The relative orientation of the surface normal of the part allows the classification of different regions of any solid into front-, back- and monotone-region [9]. The regions on the part surface are classified as front-facing, back-facing, and non-monotonic with respect to a given direction vector, referred to as a growth vector, and the normal vector according to the following criterion:

*Case 1:* Surface  $S$  is classified as the back-facing region if  $\hat{r} \cdot \hat{n}(p) < 0$  for all  $p \in S$ .

*Case 2:* Surface  $S$  is classified as the front-facing region if  $\hat{r} \cdot \hat{n}(p) \geq 0$  for all  $p \in S$ .

*Case 3:* Surface  $S$  is classified as non-monotonic if  $S$  includes both front-facing and back-facing points.

The front-facing, back-facing, and non-monotonic surfaces are bounded by the silhouette curves of the surfaces with respect to the  $\hat{r}$ -vector. The silhouette curve is the curve formed by all the points  $p$ , for which the surface normal vector at the point is orthogonal to the direction vector expressed mathematically as

$$\hat{r} \cdot \hat{n}(p) = 0. \quad (30)$$

The silhouette contour may consist of one or more closed curves [9]. For well-defined freeform surfaces, the normal vector, and, hence the silhouette curve is well defined. The sharp edges of the solid model correspond to the locus of all the points for which the gradient of the direction vector is undefined. Along the sharp edges of the solid model, however, the surface normal vector is undefined. All the sharp edges that have a front-facing region and a back-facing region or vice-versa adjacent to them are also included in the set of silhouette curves. A silhouette curve is further subdivided into a set of edges classified as a convex boundary silhouette edge and concave boundary silhouette edge [9]. The convex boundary silhouette edge is the silhouette curve formed along a continuous convex surface such that the surfaces adjacent to the edge satisfy the order back-facing  $\rightarrow$  front-facing along the vector  $\hat{r}$ . Similarly the concave boundary silhouette edge satisfies the order front-facing  $\rightarrow$  back-facing along the vector  $\hat{r}$ .

Once decomposed into subregions, the orientation vector of the solid is determined by projecting the silhouette curve onto a base plane. We identify a characteristic point, the centroid of the area, for the projected silhouette curve. The relative difference in the height of the characteristic point along the silhouette and the distance along  $x$  and  $y$  coordinates on the projected plane establishes the vector for a region. A quantitative measurement of the tilt and

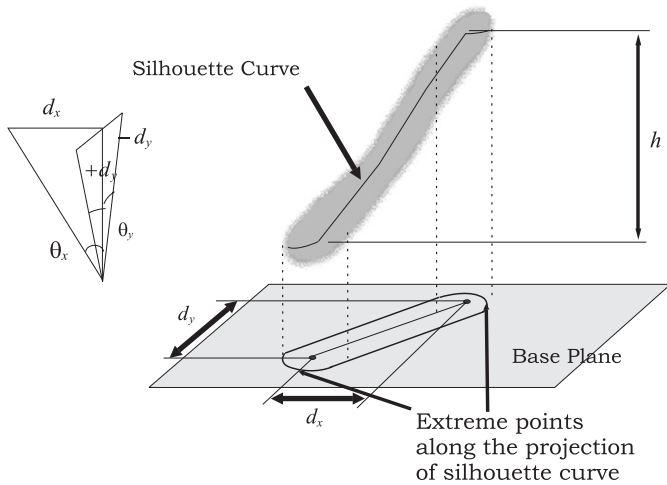


Fig. 6. Derivation of the tilt angle and the parameters for a slender structure.

rotary angle, or the desired orientation is obtained in terms of the maximum distance between the projection of two contours and the corresponding vertical distance between the two points on the curves. Parameters used for the determination of the tilt angle and the method are described in Fig. 6. The  $d_c$  is the distance along the coordinate axis  $c$  ( $c = x$  or  $y$ ) between the two projected silhouette curves. The corresponding difference of the height is  $h$ . A tilt angle defined as  $\theta_c = \arctan(d_c/h)$  is the characteristic orientation vector of the region.

For a large family of the solids, the orientation about one axis may suffice for the elimination of the support requirement; however, for certain other solids, the orientation about two axes may be required. The rotation angles about the two axes are given by

$$\theta_x = \arctan\left(\frac{d_x}{h}\right), \quad (31)$$

$$\theta_y = \arctan\left(\frac{d_y}{h}\right). \quad (32)$$

The corresponding planes of rotation are the  $xz$ -plane and the  $yz$ -plane. Where  $d_x$  and  $d_y$  correspond to the offset of silhouette curves along the  $x$ - and  $y$ - axes, respectively.

The above approach may be simplified for the slender structures based on the treatment of the solid as a freeform space trajectory and the derivation of the components of the space trajectory. The orientation of the metal deposition head with respect to the immediate deposition point is governed by the tangent vector of the curve. The subsequent adjustments made towards the choice of the orientation may be obtained by the following tangent vector:

$$\Delta \vec{v}(t) = \vec{r}(t + \Delta t) - \vec{r}(t) \quad (33)$$

as shown in the Fig. 2, where  $\Delta \vec{v}$  is the instantaneous tangent vector and  $\vec{r}(t)$  is the vector along the points on the

parametric curve that represents the space trajectory corresponding to the slender structure.

A prior analysis of the structure of the part allows decomposition of the model into different regions for the fabrication. For one set of regions, the conditions satisfied are:

$$\Delta \vec{v}(t) \cdot \hat{g} < 0, \quad (34)$$

whereas for the others it is

$$\Delta \vec{v}(t) \cdot \hat{g} \geq 0. \quad (35)$$

The prior decomposition of the solid into different regions allows a smooth variation of the machine inputs for the metal deposition.

#### 4. Experimental results and discussions

A set of experiments were performed to identify the influence of process parameters on the geometry of slender structures. The material chosen for the experiments is H13 and the argon is used as carrier medium. The relative velocity of substrate and metal deposition head, the power input, and the metal feed rate is varied, and the diameter of slender structure is measured. The results are summarized in Table 2. A trivial observation of the data suggests that the diameter increases with the increase in power and mass flow rate; whereas, it decreases on the increase in speed. A higher power allows a larger molten pool, hence, a thicker part. Similarly, the amount of material trapped in the molten pool increases with the increase in mass flow rate.

The microstructure of a slender part corresponding to the following set of input parameters is observed along the longitudinal and lateral direction of the part:

- Power = 350 W.
- Metal feed rate = 15 g/min.
- Speed of metal deposition head = 0.5 mm/s.

Table 2  
Variation of the structure diameter based on various process parameters

Power (W)	Speed (mm/s)	Mass flow (g/min)	Diameter (mm)
200	0.75	10	2.21
200	1	15	2.15
200	0.5	15	2.34
250	0.75	10	2.57
250	1	15	2.41
250	0.5	15	2.63
300	0.75	10	2.77
300	1	15	2.68
300	0.5	15	3.08
350	1	15	3.15
350	0.5	15	3.42
400	0.75	15	3.77
400	1	15	3.45
400	0.5	15	4.24

A set of complex parts were fabricated using the suggested approach. The microstructure of parts is fully dense (Fig. 7) and do not require support for fabrication.

Fig. 8 shows a spherical spiral part fabricated along a non-linear space curve defined by the following equation:

$$\begin{cases} x = \cos t \cos c \\ y = \sin t \cos c, \\ z = -\sin c \end{cases} \quad (36)$$

Where parameter  $c = \tan^{-1}\alpha t$  defines the geometry of the spiral and  $\alpha$  is a constant. The discretization of the geometry is eliminated by the coordinated motion of the

manipulation platform and the laser deposition head. Fig. 9 shows a linear slender structure with a varying cross-sectional area. The cross-sectional area of the part is varied by varying the process parameters. As observed in the figure, it is possible to shift from the underlying smaller cross-section area to a larger area and vice-versa; therefore, the process is apparently independent of the size of the underlying substrate.

Similarly, the part shown in Fig. 10 is made of branched segments fabricated by a set of linear curves in space. Contrary to the part shown in Fig. 8, which is made along a continuous curve in the space, this part comprises five distinct regions each with different orientation vector.

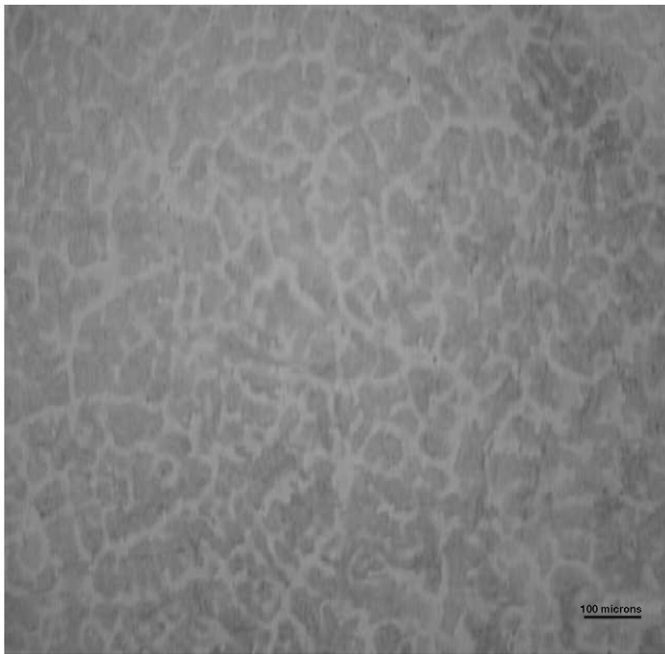


Fig. 7. Microstructure of a slender structure (parameters used to fabricate the slender structure: power = 350 W, metal feed rate = 15 g/min, speed of metal deposition head = 0.5 mm/s).

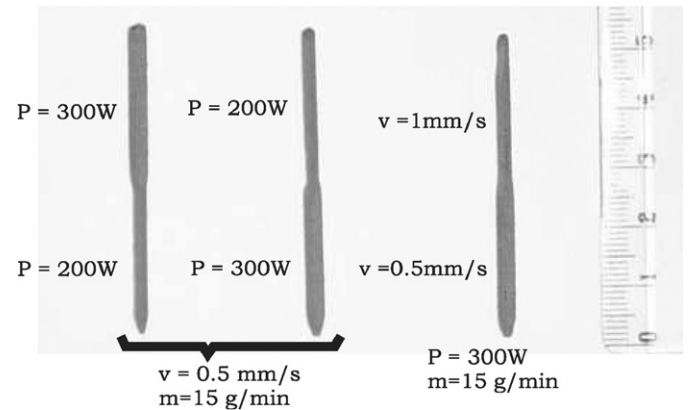


Fig. 9. Linear slender structures with varying cross-sectional area.  $P$  = power in W,  $v$  = metal deposition head velocity in mm/s and  $m$  = mass flow rate in g/min.

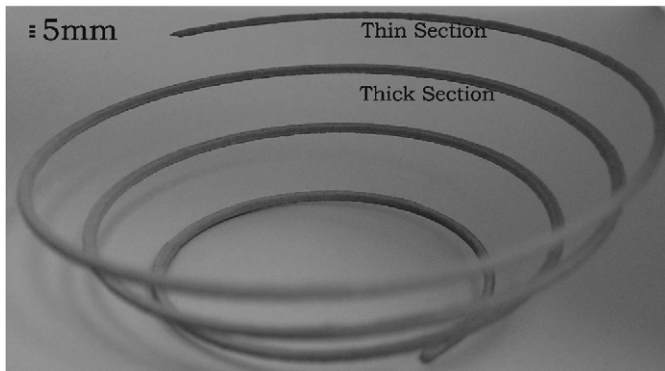


Fig. 8. Spherical fabricated by laser-based direct metal deposition. The variation in the diameter of different regions is done by varying the process parameters.



Fig. 10. A branched structure with linear segments fabricated by laser-based direct metal deposition.

## 5. Conclusions and discussions

A mathematical model is suggested for the process planning for fabrication of slender structures. The mathematical model suggests a framework for the implementation of the process and part fabrication for extremely complex parts including overhangs, which are otherwise difficult to make.

Experiments were performed in order to determine the optimal value of process parameters such as metal deposition head speed, power, and mass flow rate. Another set of numerical simulations and experiments were performed to determine the maximum molten pool volume for the inclination angle of the molten pool.

A set of complex geometries were successfully fabricated. Experiments suggest that it is possible to control the size of the cross-sectional area of the structures by varying the process parameters. The microstructure of the part obtained is uniform and dense. The LBDMD process, therefore, is a very effective method for the fabrication of complex slender structures.

## Acknowledgments

This work was financially supported by the NSF (National Science Foundation) Grants DMI-0320663. Authors would like to acknowledge the help from Mr. Michael Valant, Research Engineer and Dr. Dichao Lin, graduate student at Research Centre for Advanced Manufacturing.

## References

- [1] Laser additive machine, product details. <[http://www.optomec.com/site/lens\\_5](http://www.optomec.com/site/lens_5)>.
- [2] R. Kovacevic, Will we use welding technology to make prototypes, *SME's Manufacturing Engineering Magazine* 35B (4) (2001) 26–27.
- [3] K. Hartman, R. Krishnan, R. Merz, G. Neplotnik, F. B. Prinz, L. Schultz, M. Terk, and L. Weiss. Robot-assisted shape deposition manufacturing, in: *Proceedings of the 1994 IEEE International Conference on Robotics and Automation (ICRA '94)*, vol. 4, May 1994, pp. 2890–2895.
- [4] D. Shi, I. Gibson, Improving surface quality of selective laser sintered rapid prototype parts using robotic finishing, *Proceedings of the Institution of Mechanical Engineers Part B-Journal of Engineering Manufacture* 214 (3) (2000) 197–203.
- [5] Rapid prototyping primer. <<http://www.mne.psu.edu/lamancusa/rapidpro/primer/chapter2.htm>>.
- [6] Robocasting : Joe cesarano develops breakthrough way of fabricating ceramics. <[http://www.sandia.gov/LabNews/LN01-29-99/lens\\_story.htm](http://www.sandia.gov/LabNews/LN01-29-99/lens_story.htm)>.
- [7] P. Singh, D. Dutta, Multi-direction slicing for layered manufacturing, *Journal of Computing and Information Science and Engineering* 2 (2001) 129–142.
- [8] Hw-185, multi-axis laser powder fusion welding system. <[http://www.huffmancorp.com/products/laser\\_systems/HW-185.html](http://www.huffmancorp.com/products/laser_systems/HW-185.html)>.
- [9] R. Dwivedi, R. Kovacevic, Process planning for multi-directional laser-based direct metal deposition, *Proceedings of the I MECH E Part C-Journal of Mechanical Engineering Science* 219 (7) (2005) 695–707.
- [10] R. Dwivedi and R. Kovacevic, Process planning for solid freeform fabrication based on laser-additive multi-axis deposition, in: *Proceedings of the 14th Solid Freeform Fabrication Symposium*, 4–6 August 2003, Austin, TX, pp. 1–12.
- [11] P. Singh and D. Dutta, Offset slices for layered manufacturing, in: *Proceedings of the ASME DETC*, September 2002, Montreal, Canada.
- [12] Sara McMains. Double sided layered manufacturing, in: *Proceedings of the Japan–USA Symposium on Flexible Automation*, July 2002, Hiroshima, Japan, pp. 269–272.
- [13] Jae hyoung Park and David W. Rosen. Issues in process planning for laser chemical vapor deposition, in: *Proceedings of the thirteenth Solid Freeform Fabrication Symposium*, 5–7 August 2002, Austin, TX, pp. 269–272.
- [14] R. Dwivedi, R. Kovacevic, An expert system for generation of machine inputs for laser-based multi-directional metal deposition, *International Journal of Machine Tools and Manufacture* 46 (14) (2006) 1811–1822.
- [15] L.A. Jones, P.F. Mendez, D. Weiss, T.W. Eagar, Dynamic behavior of gas metal arc welding, in: *Proceedings of the Conference on Iron and Steel Technology*, Pohang, Korea, 1997.
- [16] S. Zekovic, R. Dwivedi, and R. Kovacevic. Thermo-structural finite element analysis of direct laser metal deposited thin wall structures, in: *Proceedings of the 16th Solid Freeform Fabrication Symposium*, 1–3 August 2005, Austin, TX, pp. 1–12.
- [17] S. Zekovic, R. Dwivedi, and R. Kovacevic. Numerical simulation of gas-powder flow from radially symmetric nozzles in laser-based direct metal deposition, in: *Proceedings of the 11th International Scientific Conference on the Contemporary Achievements in Mechanics, Manufacturing and Materials Science CAM3S*, 6–9 December 2005, Gliwice-Zakopane, Poland.
- [18] Theory Reference ANSYS Inc., *Fluid Flow*, Chapter 7.3—Volume of Fluid Method for Free Surface flows.
- [19] R. Kovacevic, System and method for fabricating or repairing a part, Accepted Patent Application No. 10/649,925, 2005.